On seismicity and structural style of oceanic transform faults: a field geological perspective from the Troodos ophiolite, Cyprus

Åke Fagereng and Christopher J. MacLeod

School of Earth & Ocean Sciences, Cardiff University, Park Place, CF10 3AT, Cardiff, United Kingdom

ABSTRACT

Aseismic creep accommodates the majority of displacement along active oceanic transform faults, also within their thermally defined seismogenic zone. The significant earthquakes that do occur are near periodic, and repeat in nearly constant locations. Neither of these observations is explained by current models that infer an olivine-dominated rheology and a thermally controlled seismogenic zone. In this contribution we review geological observations from the exhumed Southern Troodos Transform Fault Zone of Cyprus, and discuss their implications for seismogenesis at modern oceanic transform faults. In crustal level rocks, displacement was accommodated on discrete faults and in broad breccia zones, whereas at mantle levels the dominant structures are serpentinite mélanges overprinting rare and volumetrically minor, ductilely deformed peridotites. We speculate that the seismic style of crustal level faults depends on whether slip is localised, or distributed over a broad zone that must dilate during shear. At mantle levels, we highlight that the dominant deforming material is serpentinite, at least when – as in the case of Troodos – sufficient hydration has taken place. Our observations and inferences imply that transform fault seismicity depends on time- and strain- and permeability-dependent processes, and is governed by geological complexity at a range of scales.

INTRODUCTION

Oceanic transform fault plate boundaries may offset mid-ocean ridges by hundreds of kilometres. Because earthquake moment magnitude (*Mw*) normally scales with rupture length (Wells and Coppersmith, 1994), oceanic transform faults should therefore produce many great to giant earthquakes. However, it has long been recognised (e.g. Brune, 1968; Bird et al., 2002) that oceanic transforms host fewer, and smaller, earthquakes than predicted by magnitude-length relationships. Consequently, it has been suggested that most displacement on transform faults is accommodated by aseismic creep, accompanied by microseismicity of insignificant cumulative moment (Boettcher and Jordan, 2004). Where larger earthquakes ($M_w \geq 6.0$) do occur, they tend to repeat quasi-periodically on persistent locked fault patches (McGuire et al., 2005; Braunmiller and Nábělek, 2008; Sykes and Ekström, 2012). A picture is therefore emerging where oceanic transforms, although commonly considered lithologically and rheologically simple, appear to have a more complicated internal structure comprising locked asperities within larger, creeping regions.

To a first order the down-dip limit of transform fault seismogenesis is generally well approximated by a thermally controlled, frictional-viscous transition in olivine-rich rocks along the 600˚C isotherm, assuming a simple half-space cooling model (McKenzie et al., 2005; Boettcher et al., 2007; Braunmiller and Nábělek, 2008). However, in detail there are problems with this inference; for example, the predominantly aseismic behaviour at temperatures less than 600˚C is not consistent with the observed velocity-weakening behaviour of olivine-dominated rocks deformed in the laboratory under these conditions (Boettcher et al., 2007). A thermal control on earthquake distribution is also inconsistent with significant, along-strike variation in focal depths (Abercrombie and Ekström, 2001; McGuire et al., 2012), although numerical models that incorporate hydrothermal cooling can explain some observations of deeper seismicity (Roland et al. 2010). One hypothesis for steady-state aseismic behaviour cooler than the 600˚C isotherm is that hydration and alteration of olivine to serpentine causes velocity-strengthening slip under some conditions (Reinen et al., 1991; Moore et al., 1997; Boettcher and Jordan, 2004). Other possibilities involve the effects of fluid pressure to lower effective normal stress and enable velocity-strengthening creep (Scholz, 1998), or else that spatially variable degrees of damage may lead to heterogeneous fluid-mechanical rock properties (Roland et al., 2012; Froment et al., 2014).

To date, discussion on the seismic behaviour of transform faults has been based upon a combination of remote and ocean floor seismological observations, inferences drawn from laboratory experiments, and numerical models. Direct sampling, mostly by dredging, has informed the debate to only a limited extent (e.g. Prinz et al., 1976;

Honnorez et al., 1984). None of the above data sets can capture the nature or scale of geological variability, in 3-D, that must explain the complex and heterogeneous seismic style observed along oceanic transforms. To address this knowledge gap we consider the variability in lithology and deformation style that has been documented along the Southern Troodos Transform Fault Zone, a late Cretaceous oceanic transform fault preserved within the exhumed Troodos ophiolite of Cyprus (MacLeod and Murton, 1993; Gass et al., 1994). This ~5 km wide seafloor fault zone exposes a complexly-deformed section of mantle to oceanic crustal rocks deformed at temperatures from > 1000˚C down to ambient, preserved following uplift and erosion of the ~90 Myr old ophiolite massif. We briefly review the questions posed by geophysical observations along well-studied oceanic transforms, and critically evaluate associated geological models for fault zone structure in the light of our observations from the Troodos ophiolite.

SEISMIC COUPLING OF ACTIVE TRANSFORMS

The seismic coupling coefficient, χ, describes the fraction of plate motion, within the crustal seismogenic zone, that is accommodated seismically. Note that this use of the term 'coupling' differs from a classic use describing transmission of stresses across a fault – in this chapter, there is no inference of a direct link between degree of coupling and stress on a fault plane (cf. Wang and Dixon, 2004). A typical definition of seismic coupling is $\chi = \Sigma M_{obs} / \Sigma M_{ref}$ (Scholz, 2002), where ΣM_{obs} and ΣM_{ref} are the sums of observed and expected seismic moment, respectively. Seismic moment is defined as $M = GAu$, where G is shear modulus, A is rupture area, and u is average slip, and relates to earthquake magnitude by the relation: $Mw = (2/3) \log_{10} M - 6$ where M is measured in Nm. Typically, faults are considered as comprising areas that are either creeping ($\chi = 0$) or locked and hosting episodic earthquake slip ($\chi = 1$), so that a seismic coupling of $0 < \chi < 1$ implies that some portions of the fault are locked while others creep. Making the assumption that the base of the seismogenic zone is controlled by the 600˚C isotherm, Boettcher and Jordan (2004) estimated a global χ for oceanic transforms of 0.15 ± 0.02, in other words that only 15 % of transform displacement occurs seismically.

The dearth of seismicity on oceanic transforms was first recognized by Brune (1968), who envisaged this observation as arising from a relatively small effective seismogenic thickness – defining 'seismogenic' as zones where earthquakes nucleate.

However, this model of a fully coupled depth interval requires a seismogenic zone that is less than a kilometre thick (Bird and Kagan, 2004), and is consistent neither with the observed depth distribution of earthquake hypocentres throughout the oceanic crust and into the upper mantle (Abercrombie and Ekström, 2001; McGuire et al., 2012), nor with the rupture dimensions of large transform fault earthquakes (Abercrombie and Ekström, 2001). An alternative model is that the seismogenic zone has greater down-dip extent than the statistically determined effective seismogenic thickness, but is laterally discontinuous (Boettcher and Jordan, 2004); in other words, transforms may be regarded as comprising small seismogenic patches within predominantly aseismic faults, similar to models for predominantly creeping subduction thrusts in the 'asperity model' of Lay and Kanamori (1981).

In an example of coupling within single transform systems, Braunmiller and Nábělek (2008) report $\chi \sim 0.25$ on the Blanco Transform, which connects the Gorda and Juan de Fuca ridges in the North Pacific. Here, long, straight, mature segments are largely coupled, whereas immature fault systems are wider, more complex, and have lower degree of coupling. In comparison, the south Pacific Eltanin transform has $\chi \sim 0.1$ (Stewart and Okal, 1983), and comprises three, dominantly aseismic, *en echelon* faults containing locked zones hosting quasi-periodic events of $Mw \leq 6.4$ (Molnar et al., 1975; Sykes and Ekström, 2012). Rupture size appears determined by segment length, and an inferred 5 km deep base to the seismogenic zone (Sykes and Ekström, 2012), limiting the maximum seismic moment by limiting rupture area. Both of these examples are consistent with locked, seismogenic, patches embedded in dominantly creeping fault zones. These locked zones are persistent, and thus, there may be connections between χ and fault maturity, geometry, or material properties, but the geological nature of locked vs. creeping fault segments is not well constrained.

OBSERVATIONS FROM ACTIVE TRANSFORM FAULTS

In most instances individual transform faults are not simply composed of a single continuous lineament connecting two spreading ridge tips. A typical geometry may instead involve more than one continuous transform lineament, relayed by transtensional basins or transpressional push-ups, within a morphologically complex valley that may be >5 km wide (e.g. Searle, 1981; 1983; Fox and Gallo, 1984; Macdonald, 1986; Pockalny et al., 1988; Embley and Wilson, 1992). Intra-transform magmatism may occur (e.g. Hékinian et al., 1995). Transform valleys may be bordered by detachment faults or transverse ridges (e.g. Bonatti and Honnorez, 1976; Karson and Dick, 1983). Thermally generated bending stresses play a major role in generating topographic relief within and across transform valleys (Wessel and Haxby, 1990).

Detailed microseismic observations along some well-studied oceanic transforms illustrate their heterogeneity and have led to a number of conceptual models for transform fault seismic style (Figure 1). Along the East Pacific Rise, Mw 6 transform earthquakes repeat at 5 to 6-year intervals in persistent locked patches (McGuire et al., 2005) (Figure 1a). In western Gofar, McGuire et al. (2012) located > 20,000 microearthquakes during an ocean bottom seismometer deployment. They found that areas between locked patches host intense foreshock sequences involving thousands of microearthquakes, with depths extending a few kilometres into the upper mantle. The $6.0 \leq Mw \leq 6.2$ mainshocks, on the other hand, are confined to the crust and propagate neither into surrounding microseismically active, creeping regions, nor into the upper mantle. On the Discovery transform fault, also on the East Pacific Rise, interseismically locked patches also fail repeatedly in Mw 6.0 earthquakes constrained to the crust (McGuire, 2008) separated by microseismically active, dominantly aseismic zones ≤ 10 km long (Wolfson-Schwehr et al., 2014). The observations on the East Pacific Rise are consistent with 'single-mode' behaviour (Figure 1b), where fully locked fault patches fail in seismic events of predictable regularity, with little to no co-seismic rupture of interseismically creeping, but microseismically active surrounding material (McGuire et al., 2005; 2012).

The geological reasons for the bimodal seismic style along the East Pacific Rise are unclear. Fault bends of a few kilometres have been observed to arrest propagating Mw 6 earthquakes in continental transforms (Wesnousky, 2006). Froment et al. (2014) report a ~ 600 m bend in the Gofar transform at the boundary between the locked patch and the foreshock zone (Figure 1a), representing a much smaller geometrical irregularity than those arresting ruptures in the continents. Therefore, these authors interpret this bend to reflect an along-strike change in mechanical properties, rather than represent a geometrical rupture barrier. The nature of this variation in properties is an open question. A microseismically active creeping zone has anomalously low P-wave velocity, which could be explained by high porosity and increased pore fluid pressure (Roland et al., 2012). In this case, it is therefore possible that the foreshock zone prevents rupture propagation through dilatant hardening as the rupture front hits the high porosity rocks (Segall et al., 2010), and/or because aseismic slow-sliding of fluid-overpressured fault rocks prevents the elastic loading required for seismic slip (Segall and Rice, 1995). The S-wave velocity of the creeping zone temporarily decreased during a foreshock sequence (McGuire et al., 2012; Froment et al., 2014), interpreted as increased damage, possibly by aseismic deformation accompanying the microseismic foreshocks (McGuire et al., 2012).

Repeating sequences are also observed along the northern Mid-Atlantic Ridge, where slip rates are lower (Figure 1c). On the Charlie-Gibbs Transform, a *Mw* 7.1 earthquake in 2015 occurred at approximately the same epicentral location as a 1974 earthquake of similar magnitude, and similarly a 1998 *Mw* 6.8 event appears to repeat an event observed in 1967 (Aderhold and Abercrombie, 2016). The repeating rupture patches are not separated by any distinct geometrical barriers (Figure 1c), indicating these may also relate to along-strike variation in fault zone properties. The larger magnitudes of these events relative to repeating events on the faster Gofar-Discovery transform is consistent with a scaling relation where the maximum magnitude is proportional to $V^{-3/8}$ if V is time-averaged fault slip rate (Boettcher and Jordan, 2004). Aderhold and Abercrombie (2016) calculate that χ may be as high as 0.88 for this fault, if segments creeping in the interseismic period also accommodate some co-seismic displacement. This is consistent with serpentinised zones sliding stably at plate tectonic rates but become velocity-weakening at higher velocity (Reinen et al., 1994). Contrary to the 'single mode' model of persistent locked and creeping zones, this 'multi-mode model' (cf. Boettcher and Jordan, 2004) implies that the same area on a fault can accommodate both creep and seismic slip; i.e. locked zones are surrounded by conditionally stable materials that become velocity-weakening at elevated velocity (Figure 1d). Such time-dependent behaviour has also been observed on subduction thrusts (Zweck et al., 2002; Simons et al., 2011; Ide et al., 2011), and may arise from a velocity-dependence of friction (Dieterich, 1992), dynamic weakening by thermal pressurisation (Noda and Lapusta, 2013), or the behaviour of a tabular fault zone where a range of materials of diverse rheological/frictional properties are intermingled (Fagereng and Sibson, 2010; Collettini et al., 2011).

From the brief review presented here it is clear that many significant questions remain as to the mechanical properties and seismic behaviour of oceanic transform faults. It is evident that our knowledge of their physical properties far outstrips our understanding of the geological controls on their behaviour.

GEOLOGICAL SETTING OF THE SOUTHERN TROODOS TRANSFORM FAULT ZONE

Because of the difficulty of accessing the material that is being deformed in modern oceanic transform fault zones it will always be difficult to provide the geological ground-truthing necessary to answer the questions outlined above. An alternative approach to gaining insight into transform fault mechanics from a geological perspective is to examine a transform system preserved within exhumed ocean floor. To our knowledge the best such example lies within the Troodos ophiolite of Cyprus.

The Troodos ophiolite was formed by seafloor spreading in a small supra-subduction zone ocean basin in the Late Cretaceous (Mukasa and Ludden, 1987; Robertson et al., 2012). After formation this fragment of oceanic lithosphere experienced ~ 90˚ of anticlockwise rotation in the latest Cretaceous (Morris et al., 1990), before being underthrust and passively uplifted in the Miocene (Robertson et al., 2012). Differential uplift and preferential erosion has led to mantle rocks being exposed at the highest elevations, with progressively shallower stratigraphic units exposed at lower elevations in a simple radial pattern dipping away from Mt Olympus (Figure 2; Gass and Masson-Smith, 1963). Apart from this overall, large scale, dome structure, the ophiolite is largely intact, free of metamorphic overprint, and allows field study of all stratigraphic levels.

In marked contrast to the relatively simple domal structure of the main part of the Troodos ophiolite, the southern margin shows significant small-scale complexity in its outcrop pattern. This portion of the Troodos ophiolite, the 400 km^2 Limassol Forest Complex and adjoining Arakapas Fault Belt (Figure 2), is notable for the presence of a major ocean-floor strike-slip fault zone. At least 5 km in width and traceable for ~60 km along strike, this E-W trending fault zone is perpendicular to the overall N-S mean sheeted dyke orientation in the main part of the ophiolite (e.g. Gass et al., 1994). Overlain by undeformed ocean-floor sediments, it is generally accepted as being a fragment of an oceanic transform fault zone that was preserved within the ophiolite upon its exhumation (Moores and Vine, 1971; Simonian and Gass, 1978; Murton, 1986a; MacLeod, 1990; Gass et al., 1994). This seafloor structure has been termed the ‘Southern Troodos Transform Fault Zone’ (STTFZ) (MacLeod, 1990; Gass et al., 1994). After some debate it is now recognised as having been a dextrally-slipping structure (MacLeod and Murton, 1995).

GEOMETRY OF THE STTFZ

The Arakapas Fault Belt (AFB) is a 0.5-1.5 km wide E-W trending zone of intense dextral transcurrent faulting that separates the Limassol Forest Complex (LFC) from the main Troodos ophiolite and marks the northern margin of the STTFZ (Figure 3; Simonian and Gass, 1978, Gass et al., 1994). It forms a marked valley today that is inferred to mimic the original bathymetric depression coincident with the transform fault zone (Simonian and Gass, 1978). Within the AFB, discrete braided cataclastic fault strands separate blocks of extensively brecciated sheeted dyke complex (SDC). Irregular sequences of lava flows, intercalated with volcaniclastic sediments, lie unconformably on the SDC and fill small basins between upstanding fault blocks. These sediments are highly variable in thickness, to a maximum of ~300 m. They are dominated by mass flow breccia deposits intercalated with lava and dyke-derived clasts, finer turbiditic sequences, and ferruginous hydrothermal sediment. These observations are consistent with sediments derived by submarine erosion of fault scarps within and on the flanks of the transform fault zone. They provide evidence for local highs and lows within the transform valley at the time of deformation, but not sufficient to expose the mantle on the seafloor, at least within the preserved AFB.

The nature of the extrusive sequence in the AFB contrasts markedly with the orderly lava successions from the main Troodos ophiolite, in which volcaniclastic sediments are extremely rare. Extrusives from the AFB and LFC are highly depleted boninites derived from an extensive suite of syn-kinematic 'transform sequence' wehrlite and gabbro plutons and associated dykes intruded into the LFC mantle lithosphere (Murton 1986a; Gass et al., 1994). This intra-transform magmatism provides evidence that the STTFZ was at least locally transtensional during its active transform phase (Murton 1986a; MacLeod and Murton, 1993, 1995).

The present-day outcrop pattern of the LFC, to the south of the AFB, is far more complicated geologically, with extensive exposures of serpentinised mantle peridotites in the west and, to a lesser extent, in the northeast corner (Figure 3). Widespread transform-related deformation of the mantle section is described in the section below. Faulted blocks of plutonic rocks and SDC comprise much of the remainder of the central LFC, with extrusives preserved around its periphery (Gass et al., 1994). This complex disposition of outcrop reflects, in part, late Cretaceous and Tertiary uplift and exhumation of the LFC; however, 1:5000 scale geological mapping of the entire southern Troodos region (Figure 3; Simonian, 1975; Murton, 1986b; MacLeod, 1988; Gass et al., 1994) has allowed the uplift history to be carefully deconvolved from earlier active transform fault processes, as documented in detail elsewhere (Murton, 1986a; MacLeod, 1990; MacLeod and Murton, 1993; Gass et al., 1994). In summary, NE-SW stretching (in present coordinates) at the latest stage of its ocean-floor history put the STTFZ into transtension; this led to extensional reactivation of transform-parallel structures above a Moho-level detachment fault within the STTFZ (MacLeod, 1990). Subsequently, the LFC massif underwent differential uplift with respect to the main Troodos massif in response to subduction-related underthrusting in the Miocene (e.g. Gass et al., 1994; Robertson et al., 2012). This is manifested by reverse faults at the margins of the western LFC serpentinised peridotite body.

A southern margin to the STTFZ was recognised in the eastern LFC by MacLeod (1990), on the basis of the disappearance of interlava sediments in the extrusive section and absence of originally E-W steep structures once later tilting had been accounted for (Figure 3). This constrains the original width of the STTFZ to have been approximately 5 km. We prefer this figure to the slightly greater estimate of Murton (1986b), from the western LFC, which was made in the area complicated by Miocene thrusting. Within the southeastern corner of the LFC, south of the margin of the STTFZ, lies a domain of relatively regular axis-generated ocean crust apparently unaffected by transform deformation (Figure 3). This region must, by inference, have been formed at an 'Anti-Troodos' spreading axis on the opposite side of the STTFZ from the main Troodos complex. Most or all of the regular crustal section exposed in the LFC is inferred to have formed at the tip of the Anti-Troodos spreading axis and to have become incorporated into the transform-tectonised zone.

Dyke and fault strikes within both the Anti-Troodos domain and main Troodos massif are NE-SW (Figure 2, 3). Those to the north of the transform bend back to a N-S overall trend typical of Troodos as a whole (Figure 2). This swing of dyke and fault orientation mimics that of many modern oceanic transforms, at which ridge tips curve towards the active transform zone as a result of the local rotation of the extensional stress field (Figure 1a,c). On this basis some authors inferred sinistral movement on the transform (e.g. Moores et al., 1990; Cann et al., 2001). This however conflicts with direct geological evidence for dextral shear (MacLeod and Murton, 1995), and for palaeomagnetic studies which documented significant clockwise vertical-axis tectonic rotations in the NE-SW trending dyke domain (Bonhommet et al., 1988; Allerton and Vine, 1990; MacLeod et al., 1990; Morris et al., 1990; Gass et al., 1994). MacLeod et al. (1990) interpreted the spatial extent of the dyke swing, combined with evidence for seafloor graben formation in the Solea region (Varga and Moores, 1985; Moores et al., 1990), to show a preserved ridge-transform intersection west and north of the LFC (Figure 2). They showed that dyke rotation does not markedly increase with distance from the ridge-transform intersection, implying an early stage of distributed, rotational deformation in young weak lithosphere near the ridge, and localisation onto the main strike-slip STTFZ further from the ridge-transform intersection.

Palaeomagnetic studies from within the STTFZ itself are more limited than those to the north and south, but a reconnaissance study reported in Gass et al. (1994) found extreme clockwise rotations of ≥150° about steeply plunging axes in the SDC. Much of the SDC within the STTFZ is intensely brecciated and coherent areas with identifiable dyke margins are small (metres to tens of metres) and relatively rare (see below), hence it can be deduced that the sizes of rotating blocks were small compared to the deforming zone as a whole (tens to hundreds of metres). Supporting evidence that significant syn-magmatic rotational deformation is extensive within the active transform fault zone comes from cross-cutting sheeted dyke swarms and from transform sequence boninitic dykes intruded into the STTFZ. These show a range of orientations, from N-S to NE-SW to E-W, often cross-cutting but with a consistent anticlockwise younging sense (Murton, 1986a; MacLeod and Murton, 1993, 1995; Gass et al., 1994). MacLeod and Murton (1995) suggested that transform sequence gabbros were intruded at the margins of small (probably 100s of metres to km-sized) blocks rotating independently within the broader (~5 km-wide) STTFZ.

TRANSFORM FAULT ROCKS

The differential uplift and erosion that has affected the LFC and AFB in the 90 Myr since the formation of the Troodos ophiolite allows access to all structural levels of the original STTFZ and a unique opportunity to examine transform fault deformation mechanisms in space and time from the original seafloor down to the mantle lithosphere. We find that different lithologies and stratigraphic levels deform by profoundly different mechanisms. In this section we describe the observed fault rock types in order of inferred decreasing temperature and from deepest to shallowest.

High-temperature ductile deformation in the mantle sequence

Mantle sequence peridotites in the western LFC are harzburgites with subsidiary dunite bands/lenses. In the northeastern LFC massive dunite up to 200 m thick predominates, taken to represent part of the mantle-crust transition zone (Gass et al., 1994). Serpentinisation is near pervasive across the entire LFC, and generally obscures or destroys the original textures in the peridotites. Where well preserved the harzburgites display weak *l-s* tectonite fabrics defined macroscopically by the preferred alignment of bastite pseudomorphs after orthopyroxene or, in some instances, by chrome spinel, and/or cm-dm scale variation in the proportion of the pyroxene. In rare instances, equigranular to mosaic porphyroclastic textures are preserved in thin section. These high-temperature crystal-plastic fabrics are conventionally interpreted as having formed by solid-state viscous flow in the convecting asthenosphere, then passively frozen in during formation of the mantle lithosphere (e.g. Nicolas and Poirier, 1976; Murton, 1986a; Gass et al., 1994). The orientations of these 'asthenospheric' fabrics are variable: generally NE-trending in the western LFC and NW-trending in the northeastern LFC (Gass et al., 1994).

Steeply dipping, E-W striking planar fabrics, which would be parallel to the transform fault as a whole, are only observed in a few places; dominantly in the northernmost western LFC (Gass et al., 1994). In these instances, localised foliations are relatively intense across widths of several decimetres (Figure 4a), within shear zones that have been traced for metres to tens of metres (Murton, 1986a; Gass et al., 1994). Lineations are rarely observed, likely because of poor exposure. Although no microstructural studies have been possible because of the subsequent serpentinisation, we presume these fabrics to pseudomorph porphyroclastic textures from localised shear zones in the original peridotite. They are perhaps similar to the 'lithospheric' shear zones described from the Oman ophiolite (Ceuleneer et al., 1988). These 'lithospheric' shear zones are rare, or rarely preserved, but are important as they represent highest temperature deformation structures that can be related to transform fault activity within the LFC. It should be emphasised that no porphyroclastic peridotite mylonites with preserved, dynamically recrystallized matrix comparable to those reported elsewhere (e.g. Warren and Hirth, 2006) have been reported from the LFC. Although because of the subsequent serpentinisation and serpentinite deformation (see below) it is difficult to determine the original extent of the high temperature ductile shear zones, it is nevertheless evident that such structures played a relatively minor role in the preserved deformation history of the STTFZ.

Mafic mylonites

Mafic mylonite/ultramylonite shear zones do exist in the STTFZ but are very rare, having been recognised only in the core of the western LFC (Murton 1986a). They have previously assumed a significance greater than their abundance would merit because many display clear sinistral shear sense, initially taken as evidence in support of a sinistral shear sense for the transform fault as a whole (Murton 1986a). Broadly E-W trending, they are typically only centimetres to a few decimetres wide, extremely fine-grained and normally of greenschist (rarely amphibolite) facies. They are always spatially associated with transform sequence gabbroic intrusions, in some cases bounding parts of the plutons; significantly, most have mafic mineralogies within a serpentinised peridotite country rock. MacLeod and Murton (1995) showed they represent deformed remnants of transform sequence mafic dykes, and suggested the sinistral shear sense represented the accommodation of small-scale localised clockwise block rotations at the boundaries of intrusive bodies injected into the much broader dextral (transform fault) shear zone. These mafic mylonites are of minor significance and likely accumulated little strain within the STTFZ as a whole.

Serpentinite shear zones

Serpentinite shear zones are the principal transform-related structures in the mantle section of the STTFZ, both in the western and northeastern parts of the LFC (Figure 3). Whereas serpentinised peridotite is intensely deformed across most of the LFC mantle sequence outcrop, distinct bands of more intense shearing have been identified and are delineated in lime green in Figure 3. These discrete serpentinite shear zones typically form E-W striking, vertical features; however, they may also bound and juxtapose brittlely-deformed disrupted ocean crustal blocks inferred to have formed at the Anti-Troodos ridge axis and then been incorporated into the broader transform-tectonised zone.

Of the order of ~20 m wide on average, the serpentinite shear zones may exceptionally be up to 500 m wide, may be traced ≥ 2 km along strike directly or intermittently up to 8 km (Figure 3). They typically have poorly-defined boundaries and are very heterogeneous in internal structure (Figures 4b, c). They are tectonic mélanges, consisting of lenses ranging from centimetres to tens of metres in size and phacoidal to rounded in shape, set in an intensely foliated matrix of scaly to schistose serpentine of widely varying proportion (Figures 4b-d). Here, 'scaly' implies an anastomosing network of discrete, curviplanar surfaces bounding relatively low strain phacoids, whereas 'schistose' implies a subplanar, closely spaced (< cm), penetrative foliation.

Serpentinite shear zones contain discrete slip surfaces subparallel to the scaly to schistose fabric. S-C-C' fabrics are common and display consistent dextral shear sense on steeply dipping, E-W striking structures (MacLeod and Murton, 1995). The proportion of matrix to clasts increases progressively with increased deformation intensity, such that the highest strain serpentinite shear zones (mapped as lime green in Figure 3) consist of broad zones of finely foliated schistose serpentinite containing only isolated rounded clasts (Figure 4b-d). Clast lithology is principally harzburgite, dunite or pyroxenite derived from the original mantle sequence host rock and pervasively serpentinised, but in many localities also includes blocks of wehrlite, gabbro and dolerite from the transform intrusive suite. Many of the transform sequence wehrlite intrusives are fresh, proving the early serpentinisation of the mantle section. Undeformed dolerite dykes may also cut the shear zones, attesting to the syn-tectonic nature of the intrusions (Murton, 1986a; Gass et al., 1994). Mafic lithologies within serpentinite are rodingitised in many instances, and in the shear zones the foliated serpentinite adjacent to mafic blocks may also include tremolite. Talc has not been found, though it may have been replaced during the 90 Myr exhumation history of the LFC.

Brittle deformation of the mafic ocean crust

Extensive brittle deformation has disrupted what is inferred to have originally been a relatively regular ocean crustal section that was generated at an Anti-Troodos ridge axis and incorporated into the STTFZ. As described above, much of the present-day outcrop pattern of the crustal section, in the eastern LFC in particular, results from extensional reactivation of the originally transform-parallel structures at the latest stage of the seafloor history of the LFC. Nevertheless, the style of active transform fault deformation within the mafic crust can be discerned both from the AFB and from the variably disrupted blocks within the LFC.

Deformation is most clearly displayed within outcrops of the sheeted dyke complex. Most such outcrops are brecciated to a greater or lesser degree across the entire AFB and most of the northern LFC. The extent of disruption is commonly such that dyke margins have been obliterated entirely on a scale of hundreds of metres or more, and areas mapped as 'sheeted dyke complex' (Figure 3) are simply massive dolerite fault breccia zones (Figure 4e, f). Belts of dolerite fault breccia have been traced E-W for up to 7 km, and may be several hundreds of metres wide (MacLeod and Murton, 1993). Sheeted dyke fault breccias are composed of unsorted angular to sub-rounded fragments, with sub-millimetre to decimetre-sized, commonly polished clasts, in what is normally a strongly indurated matrix (Figure 4e). Petrographic studies have shown that breccia clasts are typically cemented by the same greenschist facies background alteration that affects the clasts themselves (Simonian and Gass, 1978; Gass et al., 1994). Disseminated sulphide mineralisation is common, which leads to oxidation and characteristic red surface alteration of outcrops. Together these observations show that pervasive flow of high-temperature fluids accompanied deformation throughout the transform-tectonised zone.

Discrete fault planes and fault zones are widespread at all levels of the ocean crust within the transform domain, though they are rarely well exposed. Their traces can nevertheless be mapped out within the AFB and shown to have the form of a braided anastomosing array on a scale of hundreds of metres (Figure 3; Simonian and Gass, 1978; Gass et al., 1994). Within the transform valley these fault zones generated an irregular seafloor of local transpressional highs and transtensional lows, the former being eroded into the latter (see above; Simonian and Gass, 1978).

Whereas many of the sheeted dyke breccia zones within the AFB and northern LFC are devoid of discrete fault planes, some faults do occur in association with the breccia zones. In these instances localised (typically centimetre-scale) gouge and/or foliated cataclasite may abut sub-planar fault surfaces that typically display low-angle slickensides. These faults may also anastomose on a metre-scale, mimicking their larger map-scale geometry.

Insights as to fault zone development and strain accommodation can be gained from the regions of NE-SW dyke strike a few kilometres to the north and south of the STTFZ itself. Within the regions affected by clockwise vertical-axis rotations associated with drag at the transform inside corner (MacLeod et al., 1990), deformation is also extensive but distributed on a metre- to tens-of-metres scale. Faults may either be transform parallel, with a normal component of displacement stepping down towards the AFB and northern LFC, or else dyke parallel. On the latter, low-angle slickensides with minor sinistral offsets may be developed on individual dyke margins in relatively low-strain lenses, surrounded by discrete surfaces with gouge and foliated cataclasite passing into indurated breccia zones, together forming an anastomosing zone of deformation distributed over a tens to hundreds of metre scale (Figure 4e). Substantial variability in dyke margin orientations on this scale suggests that significant rotational strains are associated with such deformation, fault breccia and gouge being generated to accommodate local space problems. As within the STTFZ itself, fault breccias within these dyke-parallel deformation zones tend to be strongly indurated and associated with disseminated sulphide mineralisation. Mineralisation is concentrated within the fault zones, demonstrating the strong link between fluid flow and deformation.

DISCUSSION: GEOLOGICAL CONTROLS ON TRANSFORM FAULT SEISMICITY

The observations described above highlight that transform faults comprise a range of lithological units complexly juxtaposed in three dimensions within a kilometres-wide fault zone. Although informative, conceptual models as shown in Figure 1 are therefore simplistic in their 2-D nature, and also lack information on the controls of locked vs. creeping vs. conditional frictional behaviour. Defining a thermally controlled base to the seismogenic zone is also likely to be a simplification, because variables such as composition and fluid pressure are inherently variable in time and space, as shown by the observations in the STTFZ.

Seismic style of basalts and sheeted dykes

The STTFZ illustrates a layered nature, not clearly defined by the 600˚C isotherm, but more reasonably instead by the boundary between a disaggregated mafic crust and serpentinised peridotite. Most clearly displayed in the sheeted dyke sequence, the mafic crust deformed by a combination of discrete faults and distributed fracturing (Figure 4g), leading to local development of broad breccia zones (Figure 4e, f). The end-member deformation style of relatively intact dykes displaced by discrete faults, typically developed along low-cohesion dyke margins, could be modelled as discrete fault planes in an elastic medium. As the faults are in basalt (and dolerite and gabbro), they are velocity-weakening at low temperatures of upper crustal deformation if they can be approximated by olivine aggregates (Boettcher et al., 2007), and therefore likely to create episodic earthquakes controlled by elastic loading. If fault strength and elastic loading rates are constant, these earthquakes could be periodic.

Because earthquake magnitude depends on rupture area, the length of faults (or soft-linked fault systems) and the thickness of the sheeted dyke section control the maximum earthquake magnitude that can be hosted on faults developed along dyke margins. These faults could, however, also propagate into underlying gabbro and upper mantle if conditions and material properties allow. Assuming transform earthquakes reflect elastic strain release with purely strike-slip displacement, the slip to length ratio (u/L) of an earthquake rupture equals $\Delta\sigma/G$. The definitions of M and Mw can then be combined and reorganised to express transform fault earthquake magnitude in terms of stress drop and rupture geometry:

$$10^{3/2(Mw+6)} = M = GAu = GL^2W(\Delta\sigma/G) \tag{1}$$

where W is the downdip width of the rupture and L is along-strike length.

Estimates for the thickness of dyke complexes in ophiolites and modern oceanic crust vary, both with uncertainty in data and interpretation, and between fast and slow spreading centres (e.g. Christensen and Salisbury, 1975). However, 3 km is near average, and is also the approximate combined thickness of lavas, dykes and upper gabbros in Troodos (Christensen and Salisbury, 1975; Gass et al., 1994). Static stress drop ($\Delta\sigma$) of transform fault earthquakes is typically ≤ 1 MPa (Boettcher and Jordan, 2004). A typical shear modulus, G, of 30 GPa then yields $u/L = \Delta\sigma/G \leq 3\times10^{-5}$. Mw 6.0 earthquakes like those on the Gofar transform have seismic moment of ~ 10^{18} Nm, and would according to Eq. 1 then require a fault length of 19 km if constrained to a 3 km depth interval, in Troodos restricted by the combined thickness of dykes, lavas, and upper gabbros. This is consistent with observations by McGuire et al. (2012) who define the rupture area of ~ Mw 6 earthquakes as 15-20 km long and confined to a 3 km downdip width at 3-6 km depth. These depths are inferred to be above the Moho, but may involve both sheeted dykes and underlying gabbroic rocks with similar composition and properties.

The calculation above implies that crustal earthquakes in transform faults may be constrained to slip surfaces within the dyke sequence, and possibly extensions into overlying basalts and underlying dyke-bearing gabbro. The breccia zones within the Troodos dyke sequence (Figure 4g), however, are more damaged and more porous, and lack clear, through-going fault surfaces. It is also unclear how much elastic strain can be accommodated in these rocks before failure. These zones may reflect the more mature, more damaged, fault segments proposed to exist by Froment et al. (2014). Shearing of a broad zone of poorly consolidated, granular material, as described in the brecciated dyke complex in Troodos, would typically be strain hardening as shear involves dilatancy, and therefore also velocity-strengthening and unlikely to fail in earthquakes (Marone et al., 1990). This would be consistent with damaged crustal zones separating locked patches in the Gofar transform (McGuire et al., 2012; Froment et al., 2014).

Seismic style of mantle rocks

The almost complete absence of evidence of high-temperature deformation of peridotite in the STTFZ is striking. The exposed mantle rocks are near pervasively serpentinised, and strain was accommodated almost completely by deformation of serpentinite. These observations demonstrate that penetration of water deep into the mantle lithosphere was efficient and widespread within the active transform domain.

One can envisage the serpentinisation to be a time- and strain-dependent process, implying an interplay in which increased serpentinisation allows strain localisation that in turn leads to dilation, fluid infiltration, and further increased serpentinisation. As such, serpentinite shear zones are likely to be strain-weakening on geological time scales. Such interplay between fluid flow, serpentinisation, and deformation has been investigated in several settings (e.g. Escartin et al., 1997; Pérez-Gussinyé and Reston, 2001; Wada et al., 2008; Hirth and Guillot, 2013) but warrants further exploration in the case of oceanic transform faults.

An important conclusion is that the controlling rheology throughout the mantle lithosphere within the STTFZ is serpentine, not olivine-rich peridotite; thus the controlling parameters must be those that control the behaviour of serpentinite, including the volumetric proportion and distribution of serpentine minerals.

One note of caution against over-interpreting the importance of serpentine, however, is that peridotite mylonites have been sampled from oceanic fracture zones (e.g. Jaroslow et al., 1996). Warren and Hirth (2006) have, accordingly, suggested that mylonitisation, grain size reduction, and a transition to diffusion creep in peridotite can lead to weakening along transforms. It is therefore likely that ductile lithosphere at deep levels within active transform zones can also deform by distributed flow of peridotite. This is probably the case in areas near the base of the lithosphere that are above the upper temperature stability limit of serpentine, as Warren and Hirth (2006) interpret mylonitisation and strain weakening to have occurred in the absence of water, with a small grain size maintained by pinning.

A similar mechanism may be recorded by the foliated peridotites in Troodos (Figure 4a); note, however, that these shear zones are narrow, poorly preserved, and played a minor role in accommodating strain along the dominant mapped structures within the STTFZ. Peridotite mylonites in the mantle section are typically cross-cut and obliterated by the abundant serpentinite shear zones. It is therefore likely that the deep extension of transforms creep steadily by diffusion creep in peridotite until damage and downward propagation of brittle faults allow hydration and serpentinisation. Water penetration, cooling and embrittlement of the STTFZ must therefore have occurred almost to the base of the lithosphere within the active transform fault zone, similar to that at the base of many oceanic detachment faults (MacLeod et al., 2002, Escartin et al., 2003). This interpretation is consistent with deeper seismicity along fault zones interpreted as more porous and damaged on transforms along the East Pacific Rise (to as much as 10 km below seafloor; e.g. McGuire, 2012; Froment et al., 2014; Wolfson-Schwehr et al., 2014).

A parameter that determines the strength and behaviour of the mantle and lower crust is therefore the degree of alteration, likely controlled by fluid flow paths and temperature. If fluids predominantly originate at the seafloor and percolate down, serpentine shear zones are likely down-dip continuations of faults within the overlying dyke sequence, controlled by fluid flow along these faults. If fluids have a deeper source, e.g. magmatic systems on leaky transforms, then new shear zones may initiate at depth, and their deformation control the location of overlying faults. In either case, it is likely that serpentine shear zones connect to faults in the overlying sheeted dyke complex. If this interpretation is correct, then rate-dependent behaviour of serpentine may determine whether earthquakes in the crust can propagate downwards. Similarly, serpentine frictional properties may determine whether earthquakes can initiate in the upper mantle, and potentially propagate to velocity-weakening fault rock assemblages at shallower levels.

Seismic Style of Serpentinite Shear Zones

Serpentine is likely to be present in the form of lizardite or chrysotile at low (<300˚C) temperatures, whereas the higher temperature phase antigorite is prevalent at more than 300˚C (Evans et al., 1976). At room temperature, antigorite has a frictional coefficient in excess of 0.5 and is not significantly weaker than other non-serpentine minerals (Reinen et al., 1994). However, with increasing temperature, antigorite friction decreases, to as low as 0.1 at temperatures >400˚C (Chernak and Hirth, 2010). Both lizardite and antigorite have shown a transition from velocity-strengthening at low velocities to velocity-weakening at high velocities (Reinen et al., 1994). Accordingly, serpentinite shear zones are likely to accommodate stable creep under steady-state conditions. This interpretation is supported by studies of serpentinite schistosity in the Santa Ynez fault of the San Andreas system, where microstructures imply mineral growth by a dissolution-precipitation mechanism at slow strain rates (Andreani et al., 2005).

Although generally aseismic and stably sliding at low velocities there is a possibility of unstable behaviour in serpentinite if velocity increases. The room temperature experiments of Reinen et al. (1994) implied that both lizardite and antigorite faults are unable to nucleate earthquakes, but can allow earthquake propagation as their behaviour becomes unstable at high velocities. At higher temperatures, Chernak and Hirth (2010) have shown a general velocity-strengthening behaviour of antigorite, and inferred that high temperature deformation of serpentine is likely to occur by steady creep. Kohli et al. (2011), however, demonstrated that dynamic weakening at near-seismic velocities can occur if slip is fast relative to thermal diffusion, allowing flash heating at ambient temperatures as low as 300˚C if velocity is high and slip is localised.

The range of strain rate dependent behaviours of serpentine outlined above emphasises that under most conditions, serpentinite shear zones are capable of accommodating steady creep at low shear stress. However, depending on variables including temperature, normal stress, fluid pressure, and deforming thickness, a range of behaviours can occur if velocity increases (e.g. Hirth and Guillot, 2013). The efficiency of steady creep is also dependent on the proportion of serpentine, as serpentine shear zones form progressively through alteration of olivine-rich assemblages and are typically preserved as mélanges of foliated serpentine with peridotite clasts (Figure 4b-d). As little as 9% serpentine may lower the strength of the aggregate to that of pure serpentine (Escartin et al., 2001). We observe that peridotite clasts within shear zones in the STTFZ are serpentinised although they lack the foliated structure of the surrounding matrix; therefore, serpentine shear zones are likely to be weak, even when clast dominated, but can still only control deformation if interconnected. Oceanic transform-related serpentine shear zones are yet to be described in detail over a range of scales. We do, however, speculate that a mechanism to create locked zones within creeping upper mantle is to have fault volumes where serpentinisation is incomplete. In such volumes, interseismically locked zones could represent lack of interconnected serpentine, or less alignment of serpentine crystals, and not be able to creep at plate boundary deformation rates. These zones would therefore be loaded by surrounding creep, and eventually fail as local stress reach a failure criterion (Sibson, 1980; Handy, 1990). When this happens, surrounding, creeping rocks are either going to arrest slip or be conditionally stable, depending on composition, temperature, fluid pressure, and other parameters. In the latter case, slip may propagate at seismic rate.

CONCLUSIONS

The exhumed STTFZ is an ~5 km wide tabular zone comprised of abundant sheared serpentinite mélanges overprinting rare foliated peridotites at lithospheric mantle levels, contrasting with discrete faults and broad zones of breccias within mafic, mostly doleritic, crustal level rocks. The range of rock types and the complex way in which they are juxtaposed reflects a range of deformation modes and would have generated a heterogeneous style of seismicity. We suggest that the internal structure of modern oceanic transform faults will be broadly comparable to that of the STTFZ, and hence that the seismic style of modern oceanic transforms (Figure 1) is likely to result from similar geological complexity across a range of scales.

Deformation in the crustal sequence contains two end-members: broad breccias (Figure 4e, f) and discrete faults (Figure 4g). We hypothesise that these represent aseismic and seismic deformation, respectively: although basaltic rocks are velocity weakening at crustal temperatures, distributed shear through a poorly consolidated breccia is likely to be velocity-hardening because of dilatancy. We propose that an explanation for the spatially distinct rupture areas in active transforms is that they are bounded by broad breccia zones through which slip cannot propagate at seismic rates (Figure 1b). Observations in the Charlie-Gibbs transform (McGuire et al., 2012) have suggested that creeping segments can be conditionally stable (Figure 1d), which could be possible in the above interpretation if the breccias are fluid over-pressured or sufficiently cemented to host local, discrete slip zones.

Deformation in the mantle is largely accommodated in serpentinite shear zones. These zones would typically deform by steady creep, but can host seismic slip under conditions where fast slip is sufficiently localised. Rare, locally preserved, foliated upper mantle peridotites (Figure 4a) attest to ductile, likely transform related shearing also in mantle rocks, possibly under dry conditions before fluids reached mantle depths and allowed serpentinisation.

These observations and inferences imply that transform fault seismicity depends on time- and strain- and permeability-dependent processes. Future projects that combine detailed, high-resolution passive- and active-source seismology with high resolution mapping and sampling will be necessary to refine our models and hypotheses. Further field investigations of exhumed transforms are also essential to better characterise the structures, deformation mechanisms, and compositions involved in the various styles of deformation that we document here.

ACKNOWLEDGMENTS

We acknowledge with gratitude the Director and staff of the Geological Survey Department of Cyprus for permission to work in Cyprus and for their ongoing support. We thank Bram Murton, Joe Cann and many others for helping us refine our ideas over many years, and Joao Duarte for his encouragement and patience. A. F. is supported by the European Research Council (ERC) grant agreement 715836 “MICA”.

REFERENCES

Abercrombie, R.E. and Ekström, G. (2001). Earthquake slip on oceanic transform faults. *Nature 410*, 74-77.

Aderhold, K., and Abercrombie, R.E. (2016). The 2015 Mw 7.1 earthquake on the Charlie ‐ Gibbs transform fault: Repeating earthquakes and multimodal slip on a slow oceanic transform. *Geophys. Res. Lett. 43*, 6119-6128.

Allerton, S. and Vine, F.J. (1990). Palaeomagnetic and structural studies of the southeastern part of the Troodos complex. In: Malpas, J.; Moores, E.M.; Panayiotou, A. and Xenophontos, C. (eds.) *Ophiolites: Oceanic Crustal Analogues, Proceedings of the Symposium "Troodos 87: Ophiolites and oceanic lithosphere"* (pp. 99-111) Geological Survey Department, Nicosia, Cyprus.

Andreani, M., Boullier, A.-M. and Gratier, J.-P. (2005). Development of schistosity by dissolution-crystallization in a Californian serpentinite gouge. *J. Struct. Geol. 27*, 2256-2267.

Bird, P., Kagan, Y.Y. and Jackson, D.D. (2002). Plate tectonics and earthquake potential of spreading ridges and oceanic transform faults. In Stein, S. and Freymuller, J.T. (Eds.), *Plate Boundary Zones*. Geodyn.Ser. v. 30, pp. 203-218. AGU: Washington D.C.

Bird, P., and Kagan, Y.Y. (2004). Plate-tectonic analysis of shallow seismicity: Apparent boundary width, beta, corner magnitude, coupled lithosphere thickness, and coupling in seven tectonic settings. *Bull. Seismol. Soc. America, 94*, 2380-2399.

Boettcher, M.S. and Jordan, T.H. (2004). Earthquake scaling relations for mid-ocean ridge transform faults. *J. Geophys. Res.109*, B12302.

Boettcher, M.S., Hirth, G. and Evans, B. (2007). Olivine friction at the base of oceanic seismogenic zones. *J. Geophys. Res. 112*, B01205.

Bonatti, E. and Honnorez, J. (1976). Sections of the earth's crust in the equatorial Atlantic. *J. Geophys. Res. 81*, 4104-4116.

Bonhommet, N., Roperch, P. and Calza, F. (1988). Palaeomagnetic arguments for block rotations along the Arakapas fault (Cyprus). *Geology 16,* 422-425.

Braunmiller, J. and Nábělek, J. (2008). Segmentation of the Blanco Transform Fault Zone from earthquake analysis: Complex tectonics of an oceanic transform fault. *J. Geophys. Res. 113*, B07108.

Brune, J.N. (1968). Seismic moment, seismicity, and rate of slip along major fault zones. *J. Geophys. Res. 73*, 777-784.

Cann J.R., Prichard H.M., Malpas J.G. and Xenophontos C. (2001). Oceanic inside corner detachments of the Limassol Forest area, Troodos ophiolite, Cyprus. *J. Geol. Soc. London 158*, 757-767.

Ceuleneer, G., Nicolas, A. and Boudier, F. (1988). Mantle flow patterns at an oceanic spreading centre: the Oman peridotites record. *Tectonophys. 151*, 1-26.

Chernak, L.J. and Hirth, G. (2010). Deformation of antigorite serpentinite at high temperature and pressure. *Earth Planet. Sci. Lett. 296*, 23-33.

Christensen, N.I. and Salisbury, M.H. (1975). Structure and constitution of the lower oceanic crust. *Rev. Geophys. 13*, 57–86.

Collettini, C., Niemeijer, A., Viti, C., Smith, S.A. and Marone, C. (2011). Fault structure, frictional properties and mixed-mode fault slip behavior. *Earth Planet. Sci. Lett. 311*, 316-327.

Dieterich, J.H. (1992). Earthquake nucleation on faults with rate-and state-dependent strength. *Tectonophysics 211*, 115-134.

Embley, R.W., Wilson, D.S. (1992). Morphology of the Blanco Transform Fault Zone-NE Pacific: Implications for its tectonic evolution. *Marine Geophysical Researches 14*, 25-45.

Escartin, J., Hirth, G. and Evans, B. (1997). Effects of serpentinization on the lithospheric strength and the style of normal faulting at slow-spreading ridges. *Earth Planet. Sci. Lett. 151*, 181-189.

Escartin, J., Hirth, G., and Evans, B. (2001). Strength of slightly serpentinized peridotites: Implications for the tectonics of oceanic lithosphere. *Geology 29*, 1023-1026.

Escartín, J., Mével, C., MacLeod, C.J. and McCaig, A.M. (2003). Constraints on deformation conditions and the origin of oceanic detachments: the Mid-Atlantic Ridge core complex at 15°45'N. *Geochem., Geophys., Geosys. 4 (8)*, doi:10.1029/2002GC000472, 37pp.

Evans, B.W., Johannes, H., Oterdoom, H. and Trommsdorff, V. (1976). Stability of chrysotile and antigorite in the serpentine multisystem. *Schweiz. Miner. Petrogr. Mitt. 56*, 79-93.

Fagereng, Å., and Sibson, R. H. (2010). Melange rheology and seismic style. *Geology 38*, 751-754.

Fox, P.J. and Gallo, D.G. (1984). A tectonic model for ridge-transform-ridge plate boundaries: Implications for the structure of oceanic lithosphere. *Tectonophysics 104*, 205-242.

Froment, B., McGuire, J.J., Hilst, R.D., Gouédard, P., Roland, E.C., Zhang, H. and Collins, J.A. (2014). Imaging along-strike variations in mechanical properties of the Gofar transform fault, East Pacific Rise. *J. Geophys. Res. 119*, 7175-7194.

Gass, I.G., MacLeod, C.J., Murton, B.J., Panayiotou, A., Simonian, K.O. and Xenophontos, C. (1994). *The Geological Evolution of the Southern Troodos Transform Fault Zone.* Cyprus Geological Survey Memoir, **9**, Geological Survey Dept., Nicosia, Cyprus, 218pp.

Gass, I.G. and Masson-Smith, D. (1963). The Geology and Gravity Anomalies of the Troodos Massif, Cyprus, *Phil. Trans. Roy. Soc. London A255*, 417-467.

Handy, M.R. (1990). The solid-state flow of polymineralic rocks. *J. Geophys. Res. 95*, 8647-8661.

Hékinian, R., Bideau, D., Hébert, R., and Niu, Y. (1995). Magmatism in the Garrett transform fault (East Pacific Rise near 13˚27'S). *J. Geophys. Res. 100*, 10163–10185.

Hirth, G. and Guillot, S. (2013) Rheology and tectonic significance of serpentinite. *Elements 9*, 107-113.

Honnorez, J., Mével, C., and Montigny, R. (1984). Geotectonic significance of gneissic amphibolites from the Vema fracture zone, Equatorial Mid-Atlantic Ridge. *J. Geophys. Res. 89*, 11379-11400.

Ide, S., Baltay, A. and Beroza, G.C. (2011). Shallow dynamic overshoot and energetic deep rupture in the 2011 Mw 9.0 Tohoku-Oki earthquake. *Science 33*, 1426-1429.

Jaroslaw, G.E., Hirth, G. and Dick, H.J.B. (1996). Abyssal peridotite mylonites: implications for grain-size sensitive flow and strain localization in the oceanic lithosphere. *Tectonophysics 256*, 17-37.

Karson, J.A. and H.J.B. Dick (1983). Tectonics of ridge-transform intersections at the Kane Fracture Zone, 24°N on the Mid-Atlantic Ridge. *Mar. Geophys. Res. 6*, 51-98.

Kohli, A.H., Goldsby, D.L., Hirth, G. and Tullis, T. (2011). Flash weakening of serpentinite at near-seismic slip rates. *J. Geophys. Res. 116*, B03202.

Lay, T. and Kanamori, H. (1981) An asperity model of large earthquake sequences. In: *Earthquake Prediction*. Maurice Ewing Series. No.4. American Geophysical Union, pp. 579-592. ISBN 9780875904030.

Macdonald, K.C., Castillo, D.A., Miller, S.P., Fox, P.J., Kastens, K.A. and Bonatti, E. (1986). Deep‐tow studies of the Vema Fracture Zone: 1. Tectonics of a major slow slipping transform fault and its intersection with the Mid-Atlantic Ridge. *J. Geophys. Res. 91*, 3334–3354.

MacLeod, C.J. (1988). *The tectonic evolution of the Eastern Limassol Forest Complex, Cyprus.* Unpubl. PhD thesis, Open University, 231pp.

MacLeod, C.J. (1990). Role of the Southern Troodos Troodos Transform Fault in the rotation of the Cyprus microplate: evidence from the Eastern Limassol Forest Complex. In: Malpas, J.; Moores, E.M.; Panayiotou, A. and Xenophontos, C. (eds.) *Ophiolites: Oceanic Crustal Analogues, Proceedings of the Symposium "Troodos 87: Ophiolites and oceanic lithosphere"* (pp. 75-85) Geological Survey Department, Nicosia, Cyprus.

MacLeod, C.J., Allerton, S., Gass, I.G. and Xenophontos, C. (1990). Structure of a fossil ridge-transform intersection in the Troodos ophiolite. *Nature 348*, 717-720.

MacLeod, C.J., Escartín, J., Banerji, D., Banks, G.J., Gleeson, M., Irving, D.H.B., Lilly, R.M., McCaig, A.M., Niu, Y., Allerton, S., and Smith, D.K. (2002). Direct geological evidence for oceanic detachment faulting: the Mid-Atlantic Ridge, 15°45'N *Geology 30*, 879–882.

MacLeod, C.J. and Murton, B.J. (1993). Structure and tectonic evolution of the Southern Troodos Transform Fault Zone, Cyprus. In: Prichard, H.M., Alabaster, T., Harris, N.B. and Neary, C.R. (eds.) *Magmatic Processes and Plate Tectonics* (pp. 141-176) Geological Society London Special Publication No. 76.

MacLeod, C.J. and Murton, B.J. (1995). On the sense of slip of the Southern Troodos transform fault zone, Cyprus. *Geology 23*, 257-260.

Marone, C., Raleigh, C.B. and Scholz, C. (1990). Frictional behavior and constitutive modelling of simulated fault gouge. *J. Geophys. Res. 95*, 7007–7025.

McGuire, J.J., Boettcher, M.S. and Jordan, T.H. (2005). Foreshock sequences and short-term earthquake predictability on East Pacific Rise transform faults. *Nature 434*, 457-461.

McGuire, J.J., Collins, J.A., Gouédard, P., Roland, E., Lizarralde, D., Boettcher, M.S., Behn, M.D. and Van Der Hilst, R. D. (2012). Variations in earthquake rupture properties along the Gofar transform fault, East Pacific Rise. *Nature Geoscience 5*, 336-341.

McKenzie, D.P., Jackson, J. and Priestly, K. (2005). Thermal structure of oceanic and continental lithosphere. *Earth Planet. Sci. Lett. 233*, 337-349.

Molnar, P., Atwater, T., Mammerickx, J., & Smith, S. M. (1975). Magnetic anomalies, bathymetry and the tectonic evolution of the South Pacific since the Late Cretaceous. *Geophys. J. Int. 40*, 383-420.

Moore, D. E., D. A. Lockner, S. Ma, R. Summers, and J. D. Byerlee (1997), Strengths of serpentinite gouges at elevated temperatures, *J. Geophys. Res., 102*, 14787–14801.

Moores, E.M., Varga, R.J., Verosub, K.L. and Ramsden, T.W. (1990). Regional structure of the Troodos dyke complex. In: Malpas, J.; Moores, E.M.; Panayiotou, A. and Xenophontos, C. (eds.) *Ophiolites: Oceanic Crustal Analogues, Proceedings of the Symposium "Troodos 87: Ophiolites and oceanic lithosphere"* (pp. 27-35) Geological Survey Department, Nicosia, Cyprus.

Moores, E.M. and Vine, F.J. (1971). The Troodos Massif, Cyprus and other ophiolites as oceanic crust: evaluation and implications. *Phil. Trans. Roy. Soc., Lond.* ***268***, 443-466.

Morris, A., Creer, K.M. and Robertson. A.H.F. (1990). Palaeomagnetic evidence for clockwise rotations related to dextral shear along the Southern Troodos Transform Fault (Cyprus). *Earth Planet. Sci. Lett. 99*, 250-262, 1990.

Mukasa, S.B. and Ludden, J.N. (1987). Uranium-lead isotopic ages of plagiogranites from the Troodos ophiolite, Cyprus, and their tectonic significance. *Geology 15*, 825-828.

Murton, B.J. (1986a). Anomalous oceanic lithosphere formed in a leaky transform fault: evidence from the Western Limassol Forest Complex, Cyprus. *J. Geol. Soc. London 143*, 845-854.

Murton, B.J. (1986b). *The tectonic evolution of the Western Limassol Forest Complex, Cyprus.* Unpubl. PhD thesis, Open University, 332pp.

Nicolas, A. and Poirier, J.P. (1976). *Crystalline plasticity and solid state flow in metamorphic rocks*. Wiley, New York, 444pp.

Noda, H. and Lapusta, N. (2013). Stable creeping fault segments can become destructive as a result of dynamic weakening. *Nature 493*, 518-521.

Pérez-Gussinyé, M. and Reston, T.J. (2001). Rheological evolution during extension at nonvolcanic rifted margins: onset of serpentinization and development of detachments leading to continental breakup. *J. Geophys. Res. 106*, 3961-3975.

Pockalny, R.A., Detrick, R.S. and P. J. Fox (1988). Morphology and tectonics of the Kane Transform from Sea Beam bathymetry data. *J. Geophys. Res. 93*, 3179–3193.

Prinz, M., Keil, K., Green, J.A., Reid, A.M., Bonatti, E. and Honnorez, J. (1976). Ultramafic and mafic samples from the equatorial Mid-Atlantic Ridge and fracture zones. *J. Geophys. Res. 81*, 4087-4103.

Reinen, L.A., Weeks, J.D. and Tullis, T.E. (1994). The frictional behavior of lizardite and antigorite serpentinites: Experiments, constitutive models, and implications for natural faults. *Pure Appl. Geophys. 143*, 317-358.

Robertson, A.H.F., Parlak, O. and Ustaömer, T. (2012). Overview of the Palaeozoic–Neogene evolution of Neotethys in the Eastern Mediterranean region (southern Turkey, Cyprus, Syria). *Petrol. Geosci. 18*, 381-404.

Roland, E., Lizarralde, D., McGuire, J.J. and Collins, J.A. (2012). Seismic velocity constraints on the material properties that control earthquake behavior at the Quebrada-Discovery-Gofar transform faults, East Pacific Rise. *J. Geophys. Res. 117*, B11102.

Scholz, C. H. (1998). Earthquakes and friction laws. *Nature 391*, 37-42.

Scott, C.P., Titus, S.J. and Davis J.R. (2013). Using field data to constrain a numerical kinematic model for ridge-transform deformation in the Troodos ophiolite, Cyprus. *Lithosphere 5*, 109-127.

Searle, R.C. (1981). The Active Part of the Charlie Gibbs Fracture Zone: A Study Using Sonar and Other Geophysical Techniques. *J. Geophys. Res. 86*, 243–262.

Searle, R. C. (1983). Multiple, Closely-Spaced Transform Faults in Fast-Slipping Fracture Zones. *Geology 11*, 607–610.

Segall, P., Rubin, A.M., Bradley, A.M. and Rice, J.R. (2010). Dilatant strengthening as a mechanism for slow slip events. *J. Geophys. Res. 115*, B12305.

Segall, P. and Rice, J. R. (1995). Dilatancy, compaction, and slip instability of a fluid-infiltrated fault. *J. Geophys. Res. 100*, 22155-22171.

Sibson, R.H. (1980). Transient discontinuities in ductile shear zones. *J. Struct. Geol. 2*, 165-171.

Simonian, K.O. (1975). *The geology of the Arakapas Fault Belt area, Troodos ophiolite, Cyprus.* Unpubl. PhD thesis, Open University, 151pp.

Simonian, K.O. and Gass, I.G. (1978). Arakapas fault belt, Cyprus: A fossil transform fault. *Geol. Soc. America Bulletin 89*, 1220–1230.

Simons, M., Minson, S.E., Sladen, A., Ortega, F., Jiang, J., Owen, S.E., Meng, L., Ampuero, J.-P., Wei, S., Chu, R., Helmberger, D.V., Kanamori, H., Hetland, E., Moore, A.W. and Webb, F.H. (2011). The 2011 magnitude 9.0 Tohoku-Oki earthquake: Mosaicking the megathrust from seconds to centuries. *Science 332*, 1421-1425.

Stewart, L.M. and Okal, E. A. (1983). Seismicity and aseismic slip along the Eltanin Fracture Zone. *J. Geophys. Res. 88*, 10495-10507.

Sykes, L.R. and Ekström, G. (2012). Earthquakes along Eltanin transform system, SE Pacific Ocean: Fault segments characterized by strong and poor seismic coupling and implications for long-term earthquake prediction. *Geophys. J. Int. 188*, 421-434.

Varga, R.J. and Moores, E.M. (1985). Spreading structure of the Troodos ophiolite, Cyprus. *Geology 13*, 846-850.

Wada, I., Wang, K., He, J. and Hyndman, R.D. (2008). Weakening of the subduction interface and its effects on surface heat flow, slab dehydration, and mantle wedge serpentinization. *J. Geophys. Res. 113*, B04402.

Wang, K., and Dixon, T. (2004), "Coupling" Semantics and science in earthquake research, *Eos Trans. AGU*, 85(18), 180–180.

Warren, J.M. and Hirth, J.G. (2006). Grain size sensitive deformation mechanisms in naturally deformed peridotites. *Earth Planet. Sci. Lett. 248*, 423-435.

Wells, D.L., and Coppersmith, K.J. (1994). New empirical relationships among magnitude, rupture length, rupture width, rupture area, and surface displacement. *Bull. Seismol. Soc. America 84*, 974-1002.

Wesnousky, S.G. (2006). Predicting the endpoints of earthquake ruptures. *Nature 444*, 358-360.

Wessel, P. and Haxby, W.F. (1990). Thermal stresses, differential subsidence, and flexure at oceanic fracture zones. *J. Geophys. Res. 95*, 375-391.

Wessel, P.W. Smith, H.F., Scharroo, R., Luis, J. and Wobbe, F. (2013). Generic Mapping Tools: Improved Version Released, *EOS Trans. AGU 94*, 409-410.

Wolfson-Schwehr, M., Boettcher, M.S., McGuire, J.J. and Collins, J.A. (2014). The relationship between seismicity and fault structure on the Discovery transform fault, East Pacific Rise. *Geochem., Geophys., Geosystems 15*, 3698-3712.

Zweck, C., Freymueller, J.T., and Cohen, S.C. (2002). Three-dimensional elastic dislocation modeling of the postseismic response to the 1964 Alaska earthquake. *J. Geophys. Res. 107*, doi: 10.1029/2001JB000409.

FIGURE CAPTIONS

Figure 1. Panel (a) shows the geometry and seismicity of the East Pacific Rise Transform faults, highlighting locked patches producing *Mw* 6 or greater earthquakes on the Gofar transform (patches as defined by Froment et al., 2014). Panel b) is a schematic illustration of how a 'single mode' model may explain the distribution of seismicity on the Gofar transform, following interpretations by McGuire et al. (2012). Panel (c) shows the geometry and seismicity of the Charlie-Gibbs transform, highlighting epicentres of repeating large earthquakes (after Aderhold and Abercrombie, 2016). Panel (d) depicts the 'multi-mode' model that may describe the frictional properties of a fault that fails in large earthquakes emanating from locked patches that are smaller than their rupture areas (based on descriptions and interpretations by Boettcher and Jordan (2004) and Aderhold and Abercrombie (2016)). Panels (a) and (c) were produced using Generic Mapping Tools (Wessel et al., 2013), seismic data from the ANSS database (including earthquakes ≥ *Mw* 4.0 from 1964 to 2014), and bathymetry from the GEBCO_2014 Grid, version 20150318, www.gebco.net.

Figure 2. Outline geological map of the Troodos ophiolite, Cyprus. The Solea graben is an ocean-floor extensional feature interpreted as an abandoned spreading centre. The Southern Troodos Transform Fault Zone is an E-W dextral strike-slip fault zone perpendicular to the overall N-S trend of sheeted dykes. Curvature of dyke orientations north of the transform reflects clockwise rotations, inferred to reflect drag at the inside corner of a ridge-transform intersection.

Figure 3. (a): Geological map of the Limassol Forest Complex, showing approximate limits of the Southern Troodos Transform Fault Zone and Anti-Troodos domain, after Gass et al. (1994). AFB = Arakapas Fault Belt. (b): Inset map showing detail of the scale of geological complexity within the Southern Troodos Transform Fault Zone, documented from original 1:5000 scale mapping by Simonian (1975), Murton (1986a) and MacLeod (1988).

Figure 4. (a): Well foliated E-W trending porphyroclastic fabric in peridotite, now serpentinised. Such shear zones represent the only surviving evidence for transform-

related ductile deformation in the peridotites. (b), (c) and (d): Serpentinite shear zones, showing heterogeneous nature of fabrics. The proportion of fine scaly matrix is greatest in the inferred highest strain zones (d). Such serpentinite shear zones are the dominant mode of deformation in the mantle section of the transform zone. (e), (f): Dolerite fault breccias derived from the sheeted dyke complex. Broad E-W trending belts of fault breccia are the predominant mode of deformation in the mafic ocean crustal section within the transform-tectonised zone. (g): Typical mode of deformation of sheeted dyke complex in the region 1-2 km north and south of the transform zone. Anastomosing bands of gouge and fault breccia (right) surround less deformed sheeted dykes (left). Flow of high-temperature fluids through the system gives rise to disseminated sulphide mineralisation (orange).

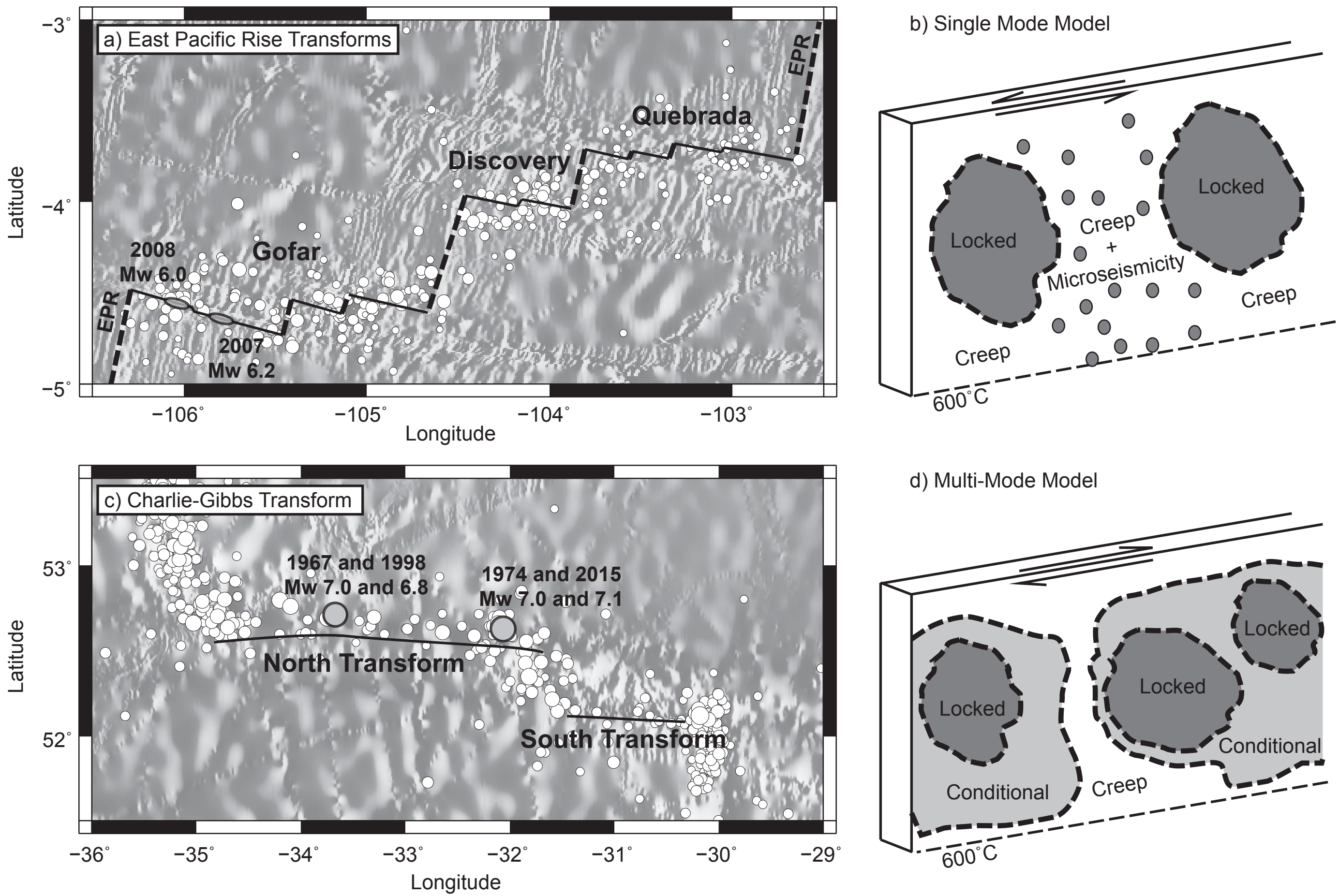

a) East Pacific Rise Transforms
EPR
Quebrada
Discovery
Gofar
2008
Mw 6.0
2007
Mw 6.2
EPR
Latitude
−3°
−4°
−5°
−106°
−105°
−104°
−103°
Longitude
b) Single Mode Model
Locked
Locked
Creep
+
Microseismicity
Creep
Creep
600°C
c) Charlie-Gibbs Transform
1967 and 1998
Mw 7.0 and 6.8
1974 and 2015
Mw 7.0 and 7.1
North Transform
South Transform
Latitude
53°
52°
−36°
−35°
−34°
−33°
−32°
−31°
−30°
−29°
Longitude
d) Multi-Mode Model
Locked
Locked
Locked
Conditional
Conditional
Creep
600°C

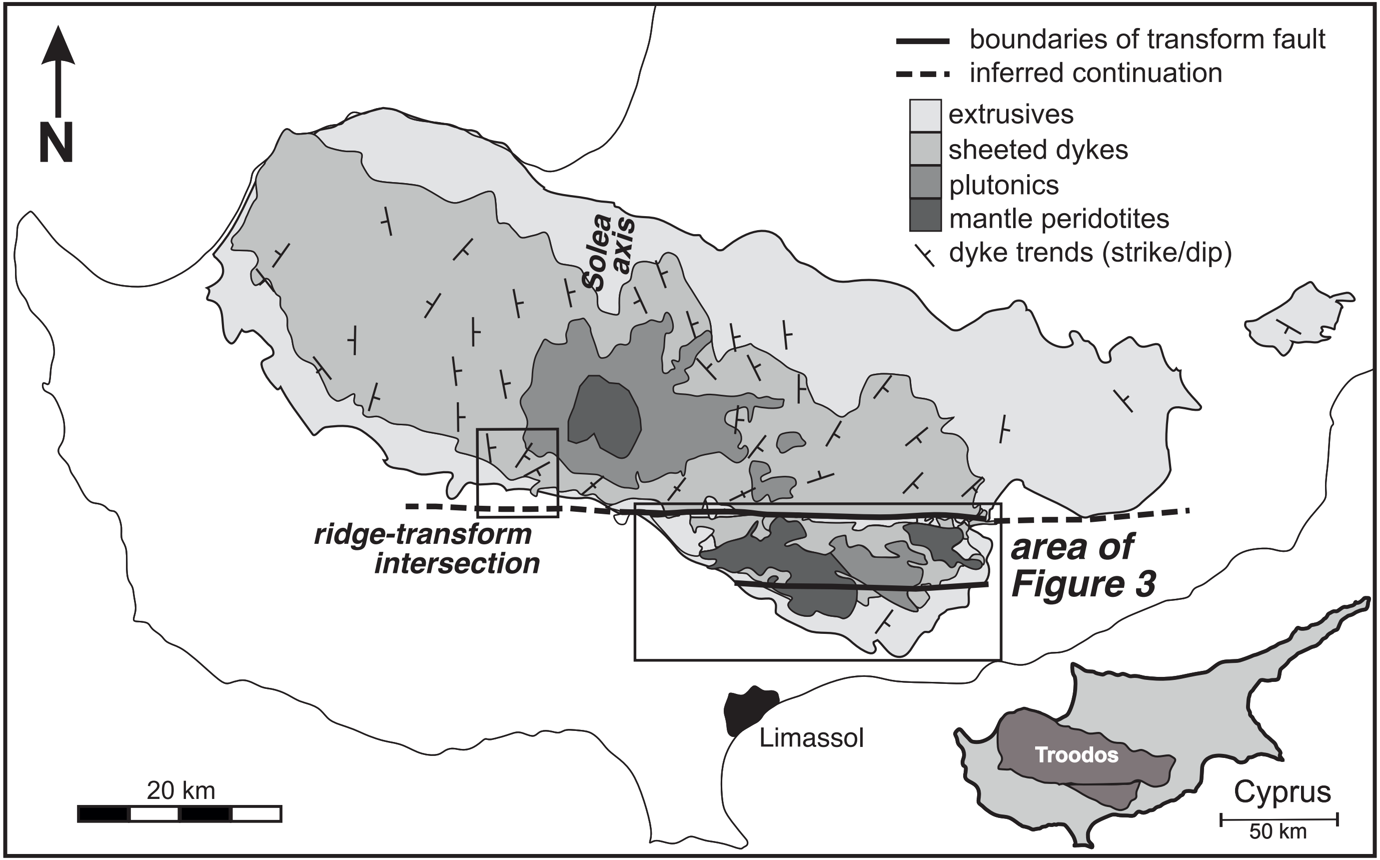

N
boundaries of transform fault
inferred continuation
extrusives
sheeted dykes
plutonics
mantle peridotites
dyke trends (strike/dip)
Solea axis
ridge-transform intersection
area of Figure 3
Limassol
Troodos
Cyprus
50 km
20 km

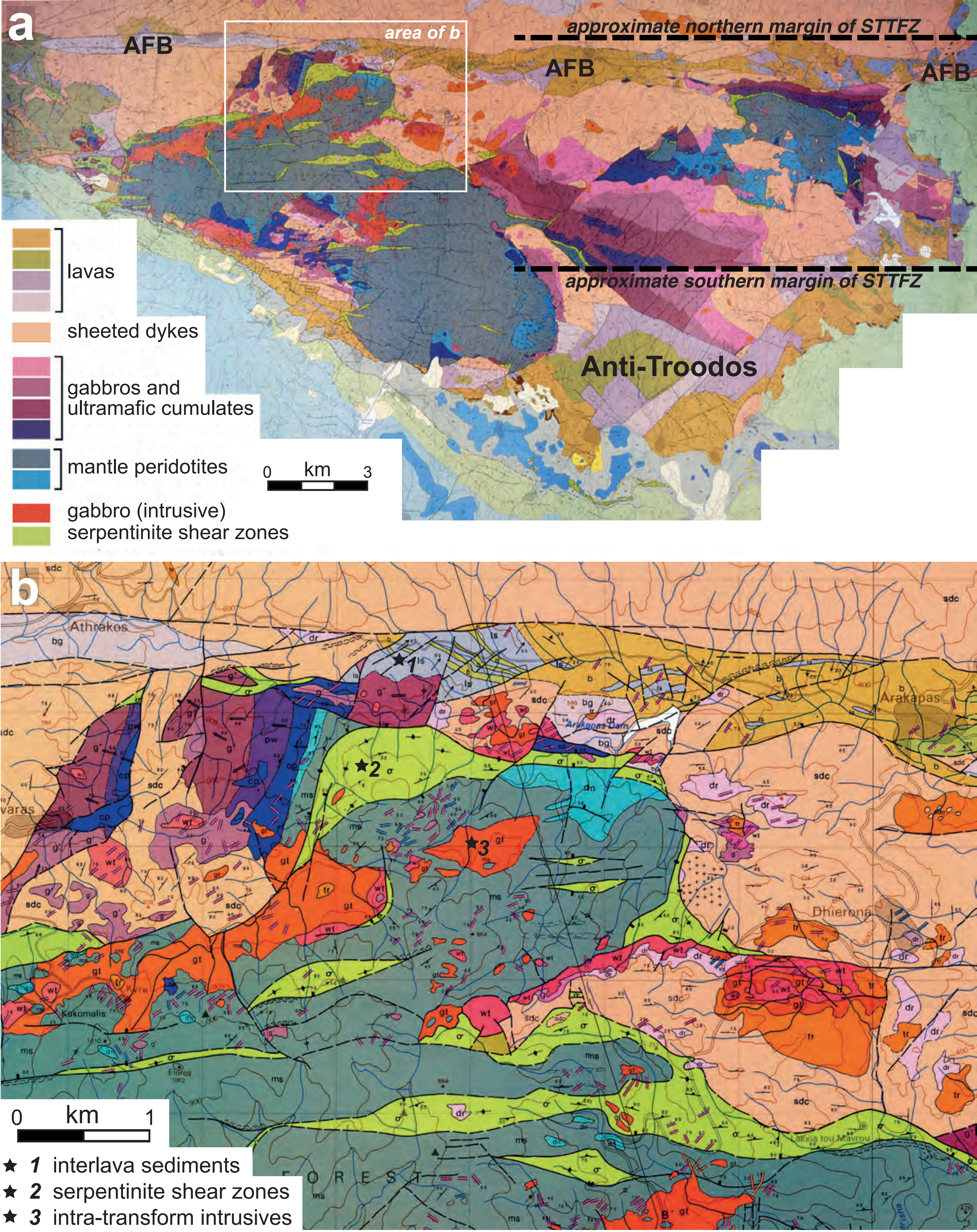
a
area of b
AFB
AFB
AFB
approximate northern margin of STTFZ
approximate southern margin of STTFZ
Anti-Troodos
lavas
sheeted dykes
gabbros and ultramafic cumulates
mantle peridotites
gabbro (intrusive)
serpentinite shear zones
0 km 3
b
Athrakos
Arakapas
Arakapas Dam
Dhierona
Kakomalis
FOREST
0 km 1
★ 1 interlava sediments
★ 2 serpentinite shear zones
★ 3 intra-transform intrusives

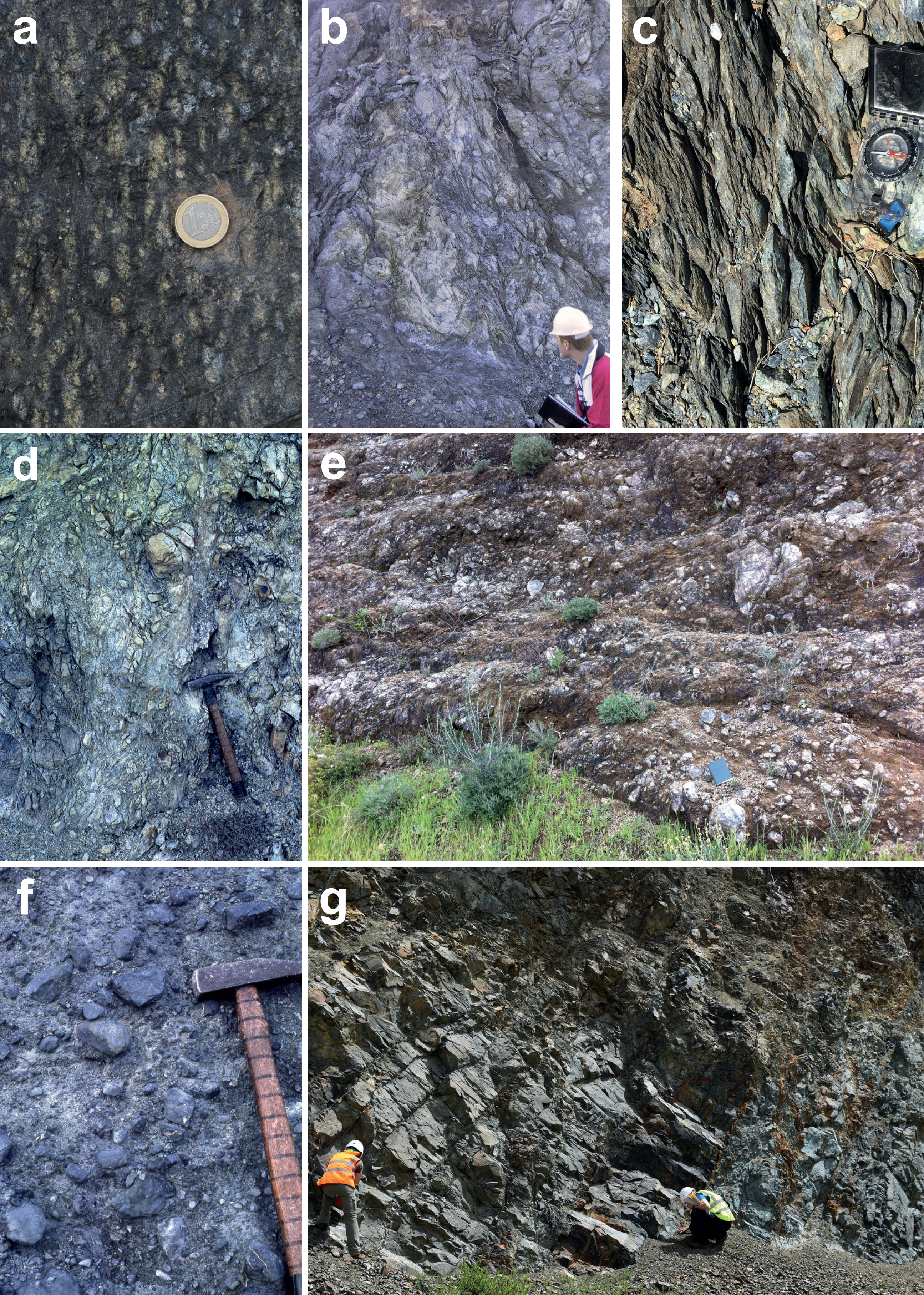
a
b
c
d
e
f
g